HHS Public Access

Author manuscript

Sci Signal. Author manuscript; available in PMC 2020 November 26.

Published in final edited form as:

Sci Signal. ; 13(633): . doi:10.1126/scisignal.aay8203.

Myeloma cells shift osteoblastogenesis to adipogenesis by inhibiting the ubiquitin ligase MURF1 in mesenchymal stem cells

Zhiqiang Liu[1,2,6,*], **Huan Liu**[1,3,6], **Jin He**[1,3], **Pei Lin**[4], **Qiang Tong**[5], **Jing Yang**[1,3,*]

[1]Department of Lymphoma and Myeloma, Center for Cancer Immunology Research, The University of Texas MD Anderson Cancer Center, Houston, Texas 77030, USA

[2]Department of Physiology and Pathophysiology, School of Basic Medical Science, Tianjin Medical University, Tianjin, China

[3]Center for Hematologic Malignancy, Research Institute Houston Methodist Hospital, Houston, Texas 77030, USA

[4]Department of Hematopathology, The University of Texas MD Anderson Cancer Center, Houston, Texas 77030, USA

[5]Children's Nutrition Research Center, Baylor College of Medicine, Houston, Texas 77030, USA

[6]These authors contribute equally to this study

Abstract

The suppression of bone formation is a hallmark of multiple myeloma. Myeloma cells inhibit osteoblastogenesis from mesenchymal stem cells (MSCs), which can also differentiate into adipocytes. We investigated myeloma-MSC interactions and the effects of such interactions on the differentiation of MSCs into adipocytes or osteoblasts using single-cell RNA sequencing, in vitro co-culture, and subcutaneous injection of MSCs and myeloma cells into mice. Our results revealed that the α4 subunit of integrin on myeloma cells stimulated vascular cell adhesion molecule 1 (VCAM1) on MSCs, leading to the activation of protein kinase C β1 (PKCβ1) signaling and repression of the muscle ring-finger protein-1 (MURF1)–mediated ubiquitylation of peroxisome proliferator-activated receptor γ2 (PPARγ2). Stabilized PPARγ2 proteins enhanced adipogenesis and consequently reduced osteoblastogenesis from MSCs, thus suppressing bone formation in vitro and in vivo. These findings reveal that suppressed bone formation is a direct consequence of myeloma-MSC contact that promotes the differentiation of MSCs into adipocytes at the expense of osteoblasts. Thus, this study provides a potential strategy for treating bone resorption in myeloma patients by counteracting tumor-MSC interactions.

[*]Corresponding authors. jyang2@houstonmethodist.org (J.Y.) and zhiqiangliu@tmu.edu.cn (Z.L.).

Author Contributions: Z.L. and J.Y. designed all experiments and wrote the manuscript; H.L., Z.L, and J.H performed all experiments and statistical analysis; P.L. provided and interpreted patient samples; Q.T. provided critical suggestions.

Conflict of interests: The authors declare that they have no competing interests.

Data and Materials Availability: All of the data needed to evaluate the conclusions in the paper are provided in the main text or the Supplementary Materials. Stable cell lines carrying targeted shRNA are available with a Materials Transfer Agreement between Houston Methodist Research Institute and the requesting institution.

Introduction

More than 80% of multiple myeloma patients suffer from bone destruction, which greatly reduces their quality of life and has a severe negative impact on survival (1). New bone formation, which usually occurs at sites of previously resorbed bone, is strongly suppressed in myeloma patients, and bone destruction rarely heals in these patients (2). Therefore, prevention of bone disease is a priority in myeloma treatment, and understanding the mechanisms by which myeloma cells disturb the bone marrow (BM) is fundamental to myeloma-associated bone diseases.

Osteoblasts originate from mesenchymal stem cells (MSCs) and are responsible for bone formation. It has been reported that myeloma cells inhibit MSC differentiation into mature osteoblasts (3–5). Osteoblasts and adipocytes arise from a common MSC-derived progenitor and exhibit lineage plasticity, which further complicates the relationship between these two cell types in myeloma cell–infiltrated BM (6). Traditionally, initiation of adipogenesis and osteogenesis has been widely regarded as mutually exclusive, and factors that inhibit osteoblastogenesis activate adipogenesis, and vice versa (7). Previous studies have demonstrated that MSCs differentiate into either adipocytes or osteoblasts depending on the stimulator (8), and adipocytes transdifferentiate into osteoblasts in patients with several benign diseases (9). However, the underlying effects of myeloma cells on the activation of adipogenic transcriptional factors and the molecular mechanisms involved are still obscure.

Peroxisome proliferator-activated receptor γ2 (PPARγ2) is a key transcription factor for the regulation of fatty acid storage and glucose metabolism (10), and it activates genes important for adipocyte differentiation and function (11). Previous findings have demonstrated that PPARγ2 plays important roles in not only the activation of adipogenesis but also in the suppression of osteoblastogenesis (12, 13). In vitro co-culture of MSCs from multiple myeloma patients with malignant plasma cell lines enhances adipocyte differentiation of the MSCs due to increased PPARγ2 in the MSCs (14), suggesting that PPARγ2 mediates myeloma-induced adipogenesis. However, the mechanism by which myeloma cells activate PPARγ2 in MSCs, thereby causing MSCs to differentiate into adipocytes rather than osteoblasts, remains unclear.

In the present study, we demonstrated that myeloma cells enhanced the differentiation of human MSCs into adipocytes rather than osteoblasts by stabilizing PPARγ2 protein through an integrin α4–protein kinase C β1 (PKCβ1)–muscle ring-finger protein-1 (MURF1) signaling pathway in MSCs. Our study thus provides a potential therapeutic strategy for myeloma-associated bone disease.

Results

Myeloma cells enhance adipogenesis and reduce osteoblastogenesis from MSCs

To determine whether myeloma cells affect MSC fate, we characterized the heterogeneity of human BM-derived MSCs after exposure to myeloma cells. We cultured MSCs alone (controls) or co-cultured them with myeloma cells in a 1:1 mixture of adipocyte:osteoblast (1:1 AD:OB) medium (Fig. 1A). An aliquot of cells was cultured for 48 hours and then

subjected to single-cell RNA sequencing (scRNA-seq). We cultured another aliquot of cells for 2 weeks, removed the myeloma cells, and assessed the ability of the MSCs to differentiate into mature osteoblasts or adipocytes using Alizarin red-S, which stains calcium deposits, and Oil red O, which stains lipids (Fig. 1A). Trajectory analysis indicated the dynamic cellular transition processes of MSCs in vitro, in line with the in vivo MSC fates, reported by Wolock *et al*. (15). Notably, we observed a fate shift in MSC differentiation when MSCs were co-cultured with myeloma cells (Fig. 1B). T-distributed stochastic neighbor embedding cluster analysis based on the entire transcriptome gene signature showed that both control and co-cultured MSCs had specific transcriptome characteristics (Fig. 1C). Following identification of genes with highly variable expression across the data set, clusters were identified in each of the control and coculture groups (Fig. 1C). Enrichment analysis demonstrated that the adipokine signaling pathway and the mineral absorption pathway were among the 20 pathways most significantly changed in MSCs co-cultured with myeloma cells (Fig. 1D). We identified clusters 0, 1, 6, and 8 in the MSCs co-cultured with myeloma cells as being of adipogenic lineage because their expression of the specific markers of adipogenesis, the *ADD1* and *PPARγ* genes, were markedly higher than that of other clusters (Fig. 1E). These results demonstrated that myeloma cells at least partially increase MSC transformation into adipocytes.

The co-culture of MSCs and myeloma cells resulted in lower Alizarin red-S staining and higher Oil red O staining in MSCs, indicating an increase in the generation of adipocytes, compared to culture of MSCs alone (Fig. 2A). We further labeled co-cultured MSCs with antibodies recognizing the osteoblast marker osteocalcin or the adipocyte marker fatty acid binding protein 4 (FABP4) and analyzed them using flow cytometry. We observed that culturing MSCs in osteoblast medium increased the osteocalcin$^+$ population and that co-culturing MSCs with myeloma cells inhibited this increase. Also, culturing MSCs in adipocyte medium increased the FABP4$^+$ population, and co-culturing them with myeloma cells further increased it. When we cultured MSCs alone in the 1:1 AD:OB medium, both the osteocalcin$^+$ and FABP4$^+$ populations increased, whereas co-culturing MSCs with myeloma cells reduced the osteocalcin$^+$ population but increased the FABP4$^+$ population (Fig 2, B to C). We obtained similar effects on osteoblastogenesis (Fig. 2D) and adipogenesis (Fig. 2E) when we co-cultured MSCs with six other myeloma cell lines or with CD138$^+$ primary myeloma cells isolated from BM aspirates from five myeloma patients, but not with plasma cells from healthy donors (Fig. 2, F to G). Real-time polymerase chain reaction (PCR) analysis further showed lower expression of the osteoblast differentiation-associated genes *alkaline phosphatase* (*ALP*), *secreted phosphoprotein 1* (*SPP1*), *collagen type I alpha 1 chain* (*COL1A1*), and *bone gamma-carboxyglutamate protein* (*BGLAP*, Fig. 2H) and higher expression of the adipocyte differentiation-associated genes *delta-like non-canonical Notch ligand 1* (*DLK1*), *diacylglycerol O-acyltransferase 1* (*DGAT1*), *FABP4*, and *fatty acid synthase* (*FASN*, Fig. 2I) in MSCs co-cultured with ARP-1 or MM.1S myeloma cells than in MSCs cultured alone. These results demonstrate that myeloma cells directed the differentiation of MSCs preferentially toward adipocytes than to osteoblasts.

Myeloma cells shift MSC differentiation through activation of PPARγ2

We next investigated the mechanism of myeloma-induced shifting of MSCs from osteoblastogenesis to adipogenesis. We focused on PPARγ2 because it is a key transcriptional factor for the activation of adipogenesis. scRNA-seq showed higher *PPARγ2* mRNA expression in MSCs co-cultured with myeloma cells compared to MSCs cultured alone (Fig. 1E). Using the co-culture system with MSCs and myeloma cells in a 1:1 mixture of adipocyte and osteoblast medium, we again observed the transformation of osteoblastogenesis into adipogenesis in MSCs co-cultured with myeloma cells (Fig. 3A), as well as an increase in the abundance of PPARγ2 in MSCs cultured with myeloma cells (Fig. 3B, fig. S1). To determine the importance of PPARγ2 in MSC transformation, we added the PPARγ2 antagonist G3335 to co-cultures. G3335 inhibited the myeloma cell–induced increase in PPARγ2 protein (Fig. 3B, fig. S1). Consistent with the Western blot results, G3335 treatment decreased Oil red O staining (Fig. 3C) and adipocyte gene expression (Fig. 3D), and increased Alizarin red-S staining (Fig. 3E) and osteoblast gene expression (Fig. 3F). These results clearly suggest that PPARγ2 mediated myeloma-induced MSC transformation into adipocytes.

Myeloma cells stimulate PPARγ2 and enhance adipogenesis from MSCs through integrin α4–VCAM1–PKCβ1 signaling

To determine whether myeloma cells distort MSC transformation through myeloma-secreted soluble factors or cell-to-cell contact, we co-cultured MSCs with ARP-1 or MM.1S myeloma cells in 1:1 AD:OB medium either together or separated by transwell inserts. We observed that the transwell co-culture had a slight effect on increased Oil red O staining, whereas cell-to-cell contact co-culture in the mixed medium produced much more significant boost of this staining, suggesting that direct interaction between MSCs and myeloma cells was needed for enhancing adipogenesis from MSCs (Fig. 4A). When we added supernatants collected from 24-hour cultures of ARP-1 or MM.1S cells to MSC cultures, we obtained results similar to those for the transwell co-culture (Fig. 4A), reaffirming the importance of direct contact of MSCs with myeloma cells.

To identify the specific molecules involved in adipocyte differentiation, we tested the effect of blocking antibodies against various integrins, which are highly expressed in myeloma cells, in co-cultures of MSCs with ARP-1 or MM.1S cells in 1:1 AD:OB medium. The addition of an antibody against integrin α4—but not antibodies against integrins α5, αV, or αL or a control IgG—markedly reduced Oil red O staining in co-cultures with both myeloma cell lines (Fig. 4B). The addition of the antibody recognizing integrin α4 to co-cultures of MSCs and ARP-1 cells in the mixed medium also increased osteoblast gene expression (Fig. 4C) and decreased adipocyte gene expression (Fig. 4D) substantially more than did the addition of the control IgG. To determine whether integrin α4 affected PPARγ2 production in MSCs, we infected ARP-1 and MM.1S cells with a lentivirus carrying short hairpin RNAs (shRNAs) targeting integrin α4 (fig. S2A). Integrin α4 knockdown (α4 KD) reduced integrin α4 production without changing the cell viability or proliferation, whereas integrin β1 remained unchanged in ARP-1 and MM.1S cells (Fig. 4E, fig S2, A to C). We also co-cultured MSCs with control or α4 KD myeloma cells in the mixed medium. Western blot analysis demonstrated that α4 KD in myeloma cells reduced PPARγ2 protein

production in MSCs more than did myeloma cells expressing a non-targeting control shRNA (Fig. 4F, fig. S2D). In addition, co-culture of MSCs with α4 KD myeloma cells induced higher Alizarin red-S staining (Fig. 4G) and osteoblast gene expression (Fig. 4H) but lower Oil red O staining (Fig. 4I) and adipocyte gene expression (Fig. 4J) compared to MSCs co-cultured with myeloma cells expressing the control shRNA.

Because vascular cell adhesion molecule 1 (VCAM1) is a major ligand of integrin α4, we investigated whether it mediated myeloma-induced MSC transformation by adding a blocking antibody against VCAM1 or control IgG to MSC and myeloma cell co-cultures. Addition of the antibody, but not IgG, increased Alizarin red-S staining (Fig. 5A) and osteoblast gene expression (Fig. 5B) but decreased Oil red O staining (Fig. 5C) and adipocyte gene expression (Fig. 5D) in MSCs. To determine whether binding of integrin α4 to VCAM1 induced an increase in PPARγ2, we constructed MSCs with reduced expression of VCAM1 using a lentivirus carrying VCAM1 shRNAs (VCAM1 KD) (Fig. 5E, fig. S3A) and co-cultured myeloma cells with control or VCAM1 KD MSCs. Western blot analysis showed that co-cultured VCAM1 KD MSCs had reduced PPARγ2 protein production compared to co-cultured MSCs expressing non-targeting control shRNA (Fig. 5F, fig. S3B). We also found that VCAM1 KD in MSCs considerably abrogated myeloma-induced suppression of osteoblastogenesis and activation of adipogenesis, because Oil red O staining and adipocyte gene expression decreased significantly (Fig 5, G to H), whereas Alizarin red-S staining and osteoblast gene expression both increased (Fig. 5, I to J).

Because VCAM1 stimulates intracellular signaling that results in the activation of protein kinase C (PKC), we examined PKC activation in co-cultures. Co-culture of myeloma cells and MSCs enhanced the phosphorylation of PKCβ1 but did not affect phosphorylation of the PKC isoforms PKCθ, PKCε, or PKCξ/λ or the abundance of total PKC, and reduced the phosphorylation of PKCα and PKCδ (Fig 6, A to B). Addition of the PKC inhibitor Go6976 to the co-cultures markedly reduced PKCβ1 phosphorylation and PPARγ2 protein in MSC cells co-cultured with ARP-1 or MM.1S cells (Fig. 6C, fig. S4). Functionally, treatment of co-cultures with Go6976 reduced Oil red O staining and increased Alizarin red-S staining (Fig. 6, D to F). Taken together, these results demonstrate that myeloma cells activated PPARγ2 in MSCs and induced MSC differentiation into adipocytes rather than osteoblasts through the integrin α4–VCAM1–PKCβ1 pathway.

Myeloma cells reduce MURF1-mediated ubiquitylation of PPARγ2 in MSCs

Because a key mechanism of regulation of PPARγ2 is its ubiquitylation-dependent proteasome-mediated degradation (16), we added the proteasome inhibitor MG132 to cultures of MSCs. We found that treatment with MG132 increased the presence of PPARγ2 protein in MSCs in a time- and dose-dependent manner (Fig. 7A, fig. S5A). MG132 treatment causes the accumulation of ubiquitylated PPARγ2 in MSCs, and co-culturing these cells with myeloma cells reduced PPARγ2 ubiquitylation (Fig. 7B, fig. S5B). However, the addition of a neutralizing antibody against VCAM1 to the co-cultures restored ubiquitylation of PPARγ2 (Fig. 7C, fig S5C.). These results suggested that myeloma cells activate PPARγ2 in MSCs through inhibition of its ubiquitylation.

To investigate the mechanism by which myeloma cells inhibited PPARγ2 ubiquitylation, we examined the E3 ubiquitin ligases known to induce ubiquitylation of PPARs (17). Among the tested ligases, we found that *MURF1* mRNA (Fig. 7D) and MURF1 protein (Fig. 7E, fig. S5D) were reduced in MSCs co-cultured with myeloma cells. Addition of the PKC inhibitor Go6976 to the co-cultures increased MURF1 protein in MSCs (Fig. 7F, fig. S5E), indicating that myeloma cells inhibited MURF1 production in MSCs through the PKC signaling pathway. Because the effects of MURF1 on PPARγ2 ubiquitylation are unclear, we examined the interaction of these two proteins in MSCs. Co-immunoprecipitation of PPARγ2 from MSCs demonstrated an interaction between MURF1 and PPARγ2 (Fig. 7G), and knockdown of MURF1 in MSCs reduced the ubiquitylation of PPARγ2 (Fig. 7H, fig S5, F to G). These results demonstrate that myeloma cells activated PPARγ2 in MSCs by reducing MURF1-mediated ubiquitylation of PPARγ2.

Myeloma cells shift MSC differentiation in vivo

To test the influence of myeloma cells on MSC differentiation in vivo, we established an extramedullary bone formation model in mice. Matrigel containing MSCs and Matrigel containing MSCs plus γ-irradiated ARP-1 cells were subcutaneously implanted into the right and left flanks of non-obese diabetic/severe combined immunodeficiency/interleukin-2rγ^{null} mice, respectively (Fig. 8A). Each sample also included human endothelial colony-forming cells (ECFCs) to stimulate blood vessel formation in the implant. In line with results of a previous study (18), we observed lower bone density in the extramedullary bones that formed in the left flanks, which were implanted with MSCs plus irradiated myeloma cells, compared to the extramedullary bones that formed on the right side, which were implanted with MSCs alone (Fig. 8A). Furthermore, we examined subcutaneous tissues on both sides of mice using histologic or immunohistochemical staining with antibodies against the mature osteoblast marker osteocalcin, the adipocyte marker perilipin, the myeloma marker CD138, and human MURF1. We observed lower numbers of new bones and osteocalcin^{+} osteoblasts and higher numbers of perilipin^{+} adipocytes in tissues on the sides of mice implanted with both MSCs and myeloma cells, reduction of MURF1 abundance in tissues on the sides of mice implanted with MSCs alone, and CD138^{+} cells only in tissues on the sides of mice implanted with myeloma cells (Fig. 8B).

We also isolated MSCs from the BM of 12 healthy human donors and 12 age-matched myeloma patients and found markedly lower *MURF1* mRNA expression in patient-derived MSCs compared to healthy donor MSCs (Fig. 8C). Western blotting validated the negative correlation between MURF1 and PPARγ2 at the protein level in MSCs isolated from 3 of 12 samples in both groups (Fig. 8D, fig. S6). When we cultured these primary MSCs in 1:1 AD:OB medium, we found lower Alizarin red-S staining and higher Oil red O staining in cultures of patient-derived MSCs than in cultures of healthy donor MSCs (Fig. 8, E to F). These findings demonstrate that myeloma cells reduced MURF1 in MSCs and skewed MSC differentiation to favor adipogenesis, resulting in the suppression of osteoblast-mediated new bone formation in myeloma-bearing mice and in cells from myeloma patients.

Discussion

Using scRNA-seq, an in vitro co-culture system, and mouse models, we demonstrated that myeloma cells shift the differentiation of MSCs into adipocytes rather than osteoblasts. Mechanistic studies revealed that integrin α4 on myeloma cells bound to VCAM1 on MSCs and inhibited ubiquitylation of PPARγ2 through PKC-MURF1 signaling. The resulting increase in PPARγ2 enhanced adipogenesis and suppressed osteoblastogenesis from MSCs. Thus, our study elucidates a previously unknown mechanism underlying myeloma-induced suppression of osteoblast-mediated bone formation and provides a potential approach for treating bone resorption in myeloma patients.

Suppressed differentiation of osteoblasts is well known to be a key reason for bone loss and skeleton-related events in myeloma patients (19). The molecules and pathways involved in myeloma-induced suppression of osteoblastogenesis include the Wnt signaling inhibitor Dickkopf-related protein 1 (DKK-1) (2, 20). However, antibody-mediated blocking of DKK-1 function cannot restore new bone formation completely or heal myeloma-induced resorbed bone, suggesting that additional factors expressed by myeloma cells critically affect bone formation. In the present study, we demonstrated that the α4 subunit of integrin, which is highly abundant in myeloma cells, promoted MSC differentiation into adipocytes, demonstrating that adhesion molecules—but not soluble factors—produced by myeloma cells primarily mediated the shift from osteoblastogenesis to adipogenesis. Integrin α4β1, also known as very late antigen-4, is a cell surface heterodimer present on malignant cells in patients with many types of cancer, including myeloma (21). It is a key adhesion molecule that acts as a receptor for the extracellular matrix protein fibronectin and the cellular receptor VCAM1. Interaction between integrin α4β1 and VCAM1 can activate mature osteoclast formation in patients with bone-metastatic breast cancer (22). In patients with multiple myeloma, this interaction promotes the secretion of interleukin-7 (IL-7) by tumor cells, which inhibits the expression of *RUNX-2*, which encodes a transcription factor that is essential for osteoblast differentiation, and RUNX-2 transcriptional regulatory activity in MSCs (23). This interaction also increases DKK-1 secretion by myeloma cells. Adding to these known mechanisms, we revealed that binding of myeloma cell integrin α4β1 to VCAM1 on the MSC surface activated the PKC signaling pathway. We also identified activation of PKCβ1, suppression of the downstream mediator MURF1, and the fundamental roles of such signaling pathways in the promotion of the MSC-derived adipocyte lineage. PKCs are also reportedly associated with Jagged-Notch signaling pathways, and they can regulate the transition of embryonic stem cells differentiating into post-mitotic neurons (24). Some immunomodulatory drugs (IMiDs), such as lenalidomide, may affect osteoblast differentiation through this pathway (25), indicating the important role of Jagged-Notch in osteoblast differentiation from MSCs. We may further investigate their impacts and mechanisms on myeloma-induced the shift of MSC fates in our next studies.

BM adipocytes are recognized as important regulators of bone remodeling rather than just being inert “filler cells” (26, 27). Normal BM adipocytes have been shown to be reprogrammed by myeloma cells and gain the ability to resorb bone in myeloma patients in remission (13). Focusing on the determination of MSC fate in this study, we investigated the molecular mechanism underlying the shift from osteoblastogenesis to adipogenesis induced

by myeloma cells. Lineage-tracing experiments have revealed that adipocytes can also originate from osterix-positive cells and are closely related to osteoblasts (28). Chan *et al* reported that BM adipocytes were derived from a progenitor cell that was also the progenitor for osteoblasts (29). Additionally, Gao *et al* reported plasticity between BM adipocytes and osteoblasts and potential transdifferentiation and transformation between these two identities after initiating differentiation (30). Despite this new knowledge about the balance between osteoblastogenesis and adipogenesis, how myeloma cells regulate this balance and transformation of MSCs is still unclear.

scRNA-seq can identify subpopulations using the transcriptome to avoid the complicated isolation procedures after cell-cell contact culture (15). We found that MSCs could be naturally divided into two populations by transcriptomic data, and at least one cluster of MSCs co-cultured with myeloma cells highly expressed adipocyte marker genes. Co-culture of myeloma cells pushed MSC differentiation toward adipocytes rather than osteoblasts, resulting in the suppression of bone formation in the in vivo extramedullary bone assay. Because MSCs are pluripotent stem cells capable of differentiation into other cell types, such as chondrocytes and skeletal muscle cells (31), whether myeloma cells affect MSC transformation into these cell types instead of osteoblasts remains unclear. Of note, it is possibile that the observed differentiation from MSC to adipocyte in the presence of myeloma cells might have been rather the result of a differentiation of MSCs into osteoblasts followed by a transdifferentiation from osteoblast into adipocyte. Further investigation is needed to address this possibility.

Like other transcription factors and co-regulators, PPARγ2 can undergo posttranslational modifications, such as phosphorylation, acetylation, and SUMOylation (32). Researchers have identified the key enzymes and target amino acid sites involved in these modifications, but modification of PPARγ2 by ubiquitylation, especially that induced by myeloma cells, is still unclear. Many E3 ligases, such as MURF1 and makorin ring finger protein 1 (MKRN1), are reported to be regulators of ubiquitylation of PPAR proteins (17, 33–35), whereas investigators have identified only polyubiquitylation at Lys^{184} and Lys^{185} (K184/185) mediated by MKRN1 (16). In the present study, we demonstrated that the E3 ligase MURF1 contributed to PPARγ2 ubiquitylation, and inhibition of MURF1 by myeloma cells reduced PPARγ2 ubiquitylation, leading to enhanced protein stability in MSCs. MURF1 contains a canonical N-terminal RING-containing E3 ligase that is required for its ubiquitin ligase activity (36). Others have reported dysregulation of MURF1 in experimental models of fasting, diabetes, cancer, denervation, and immobilization (37). However, none have reported the substrate proteins, such as PPARγ2, that are targeted for proteasomal degradation by MURF1 in patients with myeloma bone disease. Although the amino acids in PPARγ2 that MURF1 targets remain to be identified, we demonstrated that the reduced MURF1 production in MSCs induced by myeloma cells was critical for the inhibition of PPARγ2 ubiquitylation, and thus stabilization of the PPARγ2 protein. Other posttranslational modifications may also regulate PPARγ2 protein, especially SUMOylation, which was not addressed in the current study. For example, the transcriptional activity of PPARγ2 can be inhibited by SUMOylation at Lys^{107} to regulate insulin sensitivity (38), and growth differentiation factor 11 (GDF11) promotes osteoblastogenesis through enhancement of PPARγ2 SUMOylation (39). A logical next step could be the investigation of the role of

SUMOylation in myeloma-induced MSC transformation and how it interplays with the mechanisms described here.

In summary, our results shed light on the cross-talk between myeloma cells and MSCs and the impact of this interaction on the determination of the MSC-derived adipocyte lineage and the suppression of osteoblastogenesis from MSCs. Myeloma cell integrin α4 promoted phosphorylation of PKCβ1 through VCAM1, and the activated PKCβ1 reduced the production of MURF1 in MSCs, leading to reduced PPARγ2 ubiquitylation. Therefore, counteracting α4-VCAM1-MURF1–mediated adipogenesis from MSCs may be an promising strategy to heal myeloma-induced bone resorption.

Materials and Methods

Myeloma cell lines and primary myeloma cells

Myeloma cell lines ARP-1 and ARK were kindly provided by University of Arkansas for Medical Sciences (Little Rock, AR, USA), and others were purchased from ATCC. Primary myeloma cells or normal plasma cells were isolated from the bone marrow aspirates of myeloma patients or healthy donors using antibody-coated magnetic beads against CD138, respectively (Miltenyi Biotec, Inc) (40). The cells were maintained in RPMI 1640 medium with 10% fetal bovine serum. MSCs from bone marrow of healthy donors or myeloma patients were maintained and augmented in DMEM medium with 10% fetal bovine serum (13). Information of healthy donors and patients were listed in the table S1. The study was approved by the Institutional Review Board at The University of Texas MD Anderson Cancer Center.

In vitro generation of MSCs, mature adipocytes, and osteoblasts and co-culture of MSCs and myeloma cells

Human MSCs were generated from BM mononuclear cells from fetal bones of healthy human donors, characterized using flow cytometry, and labeled with antibodies against MSC markers (CD44, CD90, and CD166) (41). Mature adipocytes were generated from MSCs using an adipocyte medium, which was formulated of DMEM medium with 10% FBS, 1 μM dexamethasone, 0.2 mM indomethacin, 10 μg/ml insulin, and 0.5 mM 3-isobutyl-1-methylxanthine (41). Mature adipocytes were fixed with 4% paraformaldehyde, stained with Oil red O for 1 hour, and observed under a light microscope. Mature osteoblasts were generated from MSCs using an osteoblast medium, which was formulated of alpha MEM medium with 10% FBS, 100 nM dexamethasone, 10 mM β-glycerophosphate, and 0.05 mM L-ascorbic acid 2-phosphate (42). The bone-forming activity of osteoblasts was determined using Alizarin red-S staining (43, 44). Human MSCs were cultured alone or co-cultured with myeloma cells at a ratio of 5:1 in MSC medium, osteoblast medium, adipocyte medium, or 1:1 mixed of osteoblast and adipocyte medium with or without inhibitors (G3335 or Go6976) or neutralizing antibodies for 2 weeks. Addition of DMSO served as vehicle control for inhibitor-treatment experiments; and addition of IgG served as control for antibody-neutralizing experiments. In the Transwell non-direct contact model, adipocytes were seeded onto the bottom of culture wells and co-cultured with the myeloma cells on the insert. In direct contact co-culture system, MSCs were seeded together with the myeloma

cells in the culture wells to allow direct cell-cell contact. Supernatants collected from 24-hour cultures of myeloma cells were added to the MSCs in mixed osteoblast and adipocyte medium at a ratio of 1:5. In the experiments with primary cells, MSCs were cultured in the mixed medium for a week (45), and then co-cultured with primary myeloma cells isolated from BM aspirates from myeloma patients or normal plasma cells (PC) from BM of healthy donors for another week. Medium, inhibitors, and antibodies were refreshed every three days. After culture, the myeloma cells were removed, and the residual cells were stained with Alizarin red-S to assess osteoblast differentiation and with Oil red O to assess adipocyte differentiation. Culture of MSCs alone served as a control.

Single-cell RNA sequencing

Single-cell preparation, cDNA library synthesis, RNA sequencing, and data analysis were performed by Gene Denovo Inc. Briefly, 1×10^6 MSCs were plated for 6 hours, 5×10^6 myeloma cells were added to the MSCs directly, and the cells were co-cultured in mixed culture media for 48 hours; control MSC cells were cultured alone at the same media, and then mixed with myeloma cells at the same ratio just before preparation for analysis. After removal of dead cells, the cells in these groups were counted using a Countess II Automated Cell Counter, and the concentration was adjusted to 1000 cells/μl. The single cell suspensions were bar-coded labeled and reverse transcribed into scRNA-seq library using the Chromium Single Cell 3' GEM, Library & Gel Bead Kit (10X Genomics). The cDNA libraries from 2 independent experiments were sequenced on the Illumina HiSeq X-Ten platform and data were pooled for the analysis. Myeloma cells were excluded using CD138 markers. The raw scRNA-seq data were aligned, filtered, and normalized using Cell Ranger (10× Genomics) software (tables S2 to S6). The cell subpopulation was grouped by graph-based clustering based on the gene expression profile of each cells in Seurat (tables S7 to S8). Subsequent data analysis including standardization, cell subpopulation, difference of gene expression and marker gene screening were achieved by Seurat software.

Real-time PCR and Western blot analysis

MSCs were cultured alone or co-cultured with myeloma cells with or without G3335 or neutralizing antibodies for 48 hours. In some experiments, MG132 was added to the cultures 6 hours prior to the cell collection. Addition of DMSO served as vehicle control for inhibitor experiment; addition of IgG served as neutralizing antibody control.

Quantitative real-time PCR was performed as described (46). The primers are listed in table S9. For Western blotting, cells were lysed with 1× lysis buffer (Cell Signaling Technology), subjected to 4–20% gradient gel electrophoresis, transferred to, and immunoblotted with antibodies against integrin α4 (R&D Systems), integrin β1, VCAM1, PKC, MURF1, and phosphorylated isoforms of PKC along with p-PKC-pan (Cell Signaling Technology) and PPARγ2 (Santa Cruz Biotechnology). The membrane was stripped and re-probed with an antibody against β-actin to ensure equal protein loading, and finally signals was detected using peroxidase-conjugated secondary antibody followed by enhanced chemiluminescence system (Millipore) in the MiniChem system (Saizhi Biotech), and quantitative analysis of blots were performed using the Fiji based ImageJ software (version 1.51n, National Institute Health, Bethesda, MA, USA).

Virus packaging and lentivirus infection

Viral particles were produced by HEK293T cells transfected with PMD2G and PSPAX2 packaging plasmids (Addgene) together with lentivirus-expressing shRNA vectors targeting α4, MURF1, or VCAM1 (Sigma Aldrich). Non-targeted shRNA control (Sigma Aldrich) was used as control. Sequences for knocking down specific genes are as following: α4, 5'-CCGGGCTCCGTGTTATCAAGATTATCTCGAGATAATCTTGATAACACGGAGCTTTTT−3'; VCAM1, 5'-CCGGGGAATTAATTATCCAAGTTACCTCGAGGTAACTTGGATAATTAATTCCTTTTTTG-3'; MURF1, 5'-CCGGGAAGAGGAAGAGTCCACAGAACTCGAGTTCTGTGGACTCTTCCTCTTCTTTTTG −3' or 5'-CCGGGTATAATAATGCCTGGTCATTCTCGAGAATGACCAGGCATTATTATACTTTTTG −3'. Supernatants carrying the viral particles were harvested 48 hours later and concentrated to a 100 × volume using polyethylene glycol 8000 (Sigma Aldrich). MSCs (1×10^6 cells) were seeded 6 hours prior to the infection. Concentrated viral particles were added to MSCs or myeloma cells respectively in the presence of 8 μg/ml polybrene for 12 hours. The medium was then changed, and cells were cultured for another 48 hours until further management.

Co-immunoprecipitation and ubiquitylation assays

Cells were harvested and lysed using NP-40 lysis buffer supplemented with complete protease inhibitors, and the supernatant was precleaned with protein G beads (Thermo Fisher) and incubated with a mouse antibody against MURF1 (Santa Cruz Biotechnology) or monoclonal rabbit antibody against PPARγ2 antibody (Santa Cruz Biotechnology) at 4°C overnight with protein A/G agarose beads (Thermo Fisher). The next day, the pellet was washed four times with lysis buffer and then subjected to Western blot analysis using the antibodies against PPARγ2 or MURF1. IgG was used as a control and total cell lysates (5%) were used as input controls.

For a ubiquitylation assay, diluted lysates were incubated with an antibody against PPARγ2 at 4°C overnight after precleaning with protein G beads (Thermo Fisher). Protein G beads were added to the washed lysate/antibody mixture at 4°C for 4 hours. The resin was washed and applied to Western blot analysis using an antibody against ubiquitin.

Flow cytometry

MSCs were cultured alone or co-cultured with myeloma cells for 2 weeks. Abundance of FABP4 and osteocalcin was assessed by immunofluorescence using fluorescein isothiocyanate or APC-conjugated antibodies (BD Biosciences). After staining, cells were resuspended in phosphate-buffered saline with 1% fetal bovine serum and analyzed using a BD LSR Fortessa flow cytometer.

In vivo extramedullary bone formation

The animal experiments in the present study were approved by the MD Anderson Institutional Animal Care and Use Committee. In vivo extramedullary bone formation in non-obese diabetic/severe combined immunodeficiency/interleukin-2rγ^{null} mice was

established and examined (18). Briefly, MSCs alone or a mixture of human MSCs (1.5×10^6) and human endothelial colony-forming cells (1.5×10^6) in 0.2 ml of Matrigel (Corning Inc.) was subcutaneously injected into the right flanks of mice. This mixture and an additional 2×10^5 γ-irradiated (5000 cGy) myeloma cells were injected into the left flanks of the mice. At 8 weeks after implantation, subcutaneous tissues were established, and the mice were intraperitoneally injected with OsteoSense 750 to assess new bone formation in those tissues. The subcutaneous tissues were collected after the mice were killed and subjected to hematoxylin and eosin or immunohistochemical staining of cells labeled with an antibody against osteocalcin (a marker of mature osteoblasts), an antibody against perilipin (a marker of mature adipocytes), or an antibody against CD138 (a marker of myeloma cells).

Immunohistochemistry

The subcutaneous tissues were extracted from the mice and then formalin-fixed and paraffin-embedded. Tissue sections were deparaffinized with xylene and rehydrated to water through a graded alcohol series. Endogenous peroxidase activity was quenched with 3% hydrogen peroxide. Presence of CD138 (R&D Systems), osteocalcin, perilipin, and MURF1 (Abcam) in tissues was detected using specific antibodies. Signals were detected using secondary biotinylated antibodies and streptavidin/horseradish peroxidase. Chromagen 3,3-diaminobenzidine/H_2O_2 (Dako) was used, and slides were counterstained with hematoxylin. All slides were observed under a light microscope, and images were captured using a SPOT RT camera (Diagnostic Instruments).

Statistical analysis

Experimental values were expressed as means ± standard deviation unless indicated otherwise. Statistical significance was analyzed using the GraphPad Prism v7.0 with two tailed unpaired Student's *t*-tests for comparison of two groups, and one-way ANOVA with Tukey's multiple comparisons test for comparison of more than two groups. *P* values less than 0.05 were considered statistically significant. All results were reproduced in at least three independent experiments.

Supplementary Material

Refer to Web version on PubMed Central for supplementary material.

Acknowledgements

We thank Dr. Mulin Jun Li from Department of Genetics, Tianjin Medical University for his evaluation of our statistical analysis.

Funding: This work was supported by R01 grants from NCI (CA190863 and CA193362 to J.Y.) and by Research Scholar Grant from the American Cancer Society (127337-RSG-15-069-01-TBG to J.Y.). It was also supported by NIH/NCI (Core Labs at UT MD Anderson Cancer Center, P30CA016672) for the Small Animal Imaging and Research Histopathology Facilities.

References and Notes

1. Vallet S, Filzmoser JM, Pecherstorfer M, Podar K, Myeloma Bone Disease: Update on Pathogenesis and Novel Treatment Strategies. Pharmaceutics 10, (2018); published online EpubOct 24 (10.3390/pharmaceutics10040202).
2. Adamik J, Galson DL, Roodman GD, Osteoblast suppression in multiple myeloma bone disease. Journal of bone oncology 13, 62–70 (2018); published online EpubNov (10.1016/j.jbo.2018.09.001). [PubMed: 30591859]
3. Giuliani N, Rizzoli V, Roodman GD, Multiple myeloma bone disease: Pathophysiology of osteoblast inhibition. Blood 108, 3992–3996 (2006); published online EpubDec 15 (10.1182/blood-2006-05-026112). [PubMed: 16917004]
4. He J, Liu Z, Zheng Y, Qian J, Li H, Lu Y, Xu J, Hong B, Zhang M, Lin P, Cai Z, Orlowski RZ, Kwak LW, Yi Q, Yang J, p38 MAPK in myeloma cells regulates osteoclast and osteoblast activity and induces bone destruction. Cancer Res 72, 6393–6402 (2012); published online EpubDec 15 (10.1158/0008-5472.CAN-12-2664). [PubMed: 23066034]
5. Liu H, Liu Z, Du J, He J, Lin P, Amini B, Starbuck MW, Novane N, Shah JJ, Davis RE, Hou J, Gagel RF, Yang J, Thymidine phosphorylase exerts complex effects on bone resorption and formation in myeloma. Science translational medicine 8, 353ra113 (2016); published online EpubAug 24 (10.1126/scitranslmed.aad8949).
6. Takada I, Kouzmenko AP, Kato S, Wnt and PPARgamma signaling in osteoblastogenesis and adipogenesis. Nature reviews. Rheumatology 5, 442–447 (2009); published online EpubAug (10.1038/nrrheum.2009.137). [PubMed: 19581903]
7. Liu HY, Wu AT, Tsai CY, Chou KR, Zeng R, Wang MF, Chang WC, Hwang SM, Su CH, Deng WP, The balance between adipogenesis and osteogenesis in bone regeneration by platelet-rich plasma for age-related osteoporosis. Biomaterials 32, 6773–6780 (2011); published online EpubOct (10.1016/j.biomaterials.2011.05.080). [PubMed: 21700330]
8. Liu Y, Berendsen AD, Jia S, Lotinun S, Baron R, Ferrara N, Olsen BR, Intracellular VEGF regulates the balance between osteoblast and adipocyte differentiation. The Journal of clinical investigation 122, 3101–3113 (2012); published online EpubSep (10.1172/JCI61209). [PubMed: 22886301]
9. Savopoulos C, Dokos C, Kaiafa G, Hatzitolios A, Adipogenesis and osteoblastogenesis: trans-differentiation in the pathophysiology of bone disorders. Hippokratia 15, 18–21 (2011); published online EpubJan ([PubMed: 21607030]
10. Gorga A, Rindone GM, Regueira M, Pellizzari EH, Camberos MC, Cigorraga SB, Riera MF, Galardo MN, Meroni SB, PPARgamma activation regulates lipid droplet formation and lactate production in rat Sertoli cells. Cell and tissue research 369, 611–624 (2017); published online EpubSep (10.1007/s00441-017-2615-y). [PubMed: 28432465]
11. Abdelkarim M, Caron S, Duhem C, Prawitt J, Dumont J, Lucas A, Bouchaert E, Briand O, Brozek J, Kuipers F, Fievet C, Cariou B, Staels B, The farnesoid X receptor regulates adipocyte differentiation and function by promoting peroxisome proliferator-activated receptor-gamma and interfering with the Wnt/beta-catenin pathways. The Journal of biological chemistry 285, 36759–36767 (2010); published online EpubNov 19 (10.1074/jbc.M110.166231). [PubMed: 20851881]
12. Kawai M, Rosen CJ, PPARgamma: a circadian transcription factor in adipogenesis and osteogenesis. Nature reviews. Endocrinology 6, 629–636 (2010); published online EpubNov (10.1038/nrendo.2010.155).
13. Liu H, He J, Koh SP, Zhong Y, Liu Z, Wang Z, Zhang Y, Li Z, Tam BT, Lin P, Xiao M, Young KH, Amini B, Starbuck MW, Lee HC, Navone NM, Davis RE, Tong Q, Bergsagel PL, Hou J, Yi Q, Orlowski RZ, Gagel RF, Yang J, Reprogrammed marrow adipocytes contribute to myeloma-induced bone disease. Science translational medicine 11, (2019); published online EpubMay 29 (10.1126/scitranslmed.aau9087).
14. Ruan J, Trotter TN, Nan L, Luo R, Javed A, Sanderson RD, Suva LJ, Yang Y, Heparanase inhibits osteoblastogenesis and shifts bone marrow progenitor cell fate in myeloma bone disease. Bone 57, 10–17 (2013); published online EpubNov (10.1016/j.bone.2013.07.024). [PubMed: 23895995]
15. Wolock SL, Krishnan I, Tenen DE, Matkins V, Camacho V, Patel S, Agarwal P, Bhatia R, Tenen DG, Klein AM, Welner RS, Mapping Distinct Bone Marrow Niche Populations and Their

Differentiation Paths. Cell reports 28, 302–311 e305 (2019); published online EpubJul 9 (10.1016/j.celrep.2019.06.031). [PubMed: 31291568]

16. Kim JH, Park KW, Lee EW, Jang WS, Seo J, Shin S, Hwang KA, Song J, Suppression of PPARgamma through MKRN1-mediated ubiquitination and degradation prevents adipocyte differentiation. Cell death and differentiation 21, 594–603 (2014); published online EpubApr (10.1038/cdd.2013.181). [PubMed: 24336050]
17. Brunmeir R, Xu F, Functional Regulation of PPARs through Post-Translational Modifications. International journal of molecular sciences 19, (2018); published online EpubJun 12 (10.3390/ijms19061738).
18. Chen Y, Jacamo R, Shi YX, Wang RY, Battula VL, Konoplev S, Strunk D, Hofmann NA, Reinisch A, Konopleva M, Andreeff M, Human extramedullary bone marrow in mice: a novel in vivo model of genetically controlled hematopoietic microenvironment. Blood 119, 4971–4980 (2012); published online EpubMay 24 (10.1182/blood-2011-11-389957). [PubMed: 22490334]
19. Terpos E, Ntanasis-Stathopoulos I, Dimopoulos MA, Myeloma bone disease: from biology findings to treatment approaches. Blood 133, 1534–1539 (2019); published online EpubApr 4 (10.1182/blood-2018-11-852459). [PubMed: 30760454]
20. Feng Y, Zhang Y, Wei X, Zhang Q, Correlations of DKK1 with pathogenesis and prognosis of human multiple myeloma. Cancer biomarkers : section A of Disease markers 24, 195–201 (2019)10.3233/CBM-181909).
21. Carter RA, Wicks IP, Vascular cell adhesion molecule 1 (CD106): a multifaceted regulator of joint inflammation. Arthritis and rheumatism 44, 985–994 (2001); published online EpubMay (10.1002/1529-0131(200105)44:5<985::AID-ANR176>3.0.CO;2-P). [PubMed: 11352261]
22. Lu X, Mu E, Wei Y, Riethdorf S, Yang Q, Yuan M, Yan J, Hua Y, Tiede BJ, Lu X, Haffty BG, Pantel K, Massague J, Kang Y, VCAM-1 promotes osteolytic expansion of indolent bone micrometastasis of breast cancer by engaging alpha4beta1-positive osteoclast progenitors. Cancer cell 20, 701–714 (2011); published online EpubDec 13 (10.1016/j.ccr.2011.11.002). [PubMed: 22137794]
23. Giuliani N, Colla S, Morandi F, Lazzaretti M, Sala R, Bonomini S, Grano M, Colucci S, Svaldi M, Rizzoli V, Myeloma cells block RUNX2/CBFA1 activity in human bone marrow osteoblast progenitors and inhibit osteoblast formation and differentiation. Blood 106, 2472–2483 (2005); published online EpubOct 1 (10.1182/blood-2004-12-4986). [PubMed: 15933061]
24. Tischfield DJ, Kim J, Anderson SA, Atypical PKC and Notch Inhibition Differentially Modulate Cortical Interneuron Subclass Fate from Embryonic Stem Cells. Stem cell reports 8, 1135–1143 (2017); published online EpubMay 9 (10.1016/j.stemcr.2017.03.015). [PubMed: 28416285]
25. Bolomsky A, Schreder M, Meissner T, Hose D, Ludwig H, Pfeifer S, Zojer N, Immunomodulatory drugs thalidomide and lenalidomide affect osteoblast differentiation of human bone marrow stromal cells in vitro. Experimental hematology 42, 516–525 (2014); published online EpubJul (10.1016/j.exphem.2014.03.005). [PubMed: 24704163]
26. Fazeli PK, Horowitz MC, MacDougald OA, Scheller EL, Rodeheffer MS, Rosen CJ, Klibanski A, Marrow fat and bone--new perspectives. The Journal of clinical endocrinology and metabolism 98, 935–945 (2013); published online EpubMar (10.1210/jc.2012-3634). [PubMed: 23393168]
27. Trotter TN, Gibson JT, Sherpa TL, Gowda PS, Peker D, Yang Y, Adipocyte-Lineage Cells Support Growth and Dissemination of Multiple Myeloma in Bone. The American journal of pathology 186, 3054–3063 (2016); published online EpubNov (10.1016/j.ajpath.2016.07.012). [PubMed: 27648615]
28. Liu Y, Strecker S, Wang L, Kronenberg MS, Wang W, Rowe DW, Maye P, Osterix-cre labeled progenitor cells contribute to the formation and maintenance of the bone marrow stroma. PloS one 8, e71318 (2013)10.1371/journal.pone.0071318). [PubMed: 23951132]
29. Chan CK, Seo EY, Chen JY, Lo D, McArdle A, Sinha R, Tevlin R, Seita J, Vincent-Tompkins J, Wearda T, Lu WJ, Senarath-Yapa K, Chung MT, Marecic O, Tran M, Yan KS, Upton R, Walmsley GG, Lee AS, Sahoo D, Kuo CJ, Weissman IL, Longaker MT, Identification and specification of the mouse skeletal stem cell. Cell 160, 285–298 (2015); published online EpubJan 15 (10.1016/j.cell.2014.12.002). [PubMed: 25594184]
30. Gao B, Huang Q, Lin YS, Wei BY, Guo YS, Sun Z, Wang L, Fan J, Zhang HY, Han YH, Li XJ, Shi J, Liu J, Yang L, Luo ZJ, Dose-dependent effect of estrogen suppresses the osteo-adipogenic

transdifferentiation of osteoblasts via canonical Wnt signaling pathway. PloS one 9, e99137 (2014)10.1371/journal.pone.0099137). [PubMed: 24918446]

31. Lian JB, Stein GS, van Wijnen AJ, Stein JL, Hassan MQ, Gaur T, Zhang Y, MicroRNA control of bone formation and homeostasis. Nature reviews. Endocrinology 8, 212–227 (2012); published online EpubApr (10.1038/nrendo.2011.234).
32. van Beekum O, Fleskens V, Kalkhoven E, Posttranslational modifications of PPAR-gamma: fine-tuning the metabolic master regulator. Obesity 17, 213–219 (2009); published online EpubFeb (10.1038/oby.2008.473). [PubMed: 19169221]
33. Lee KW, Cho JG, Kim CM, Kang AY, Kim M, Ahn BY, Chung SS, Lim KH, Baek KH, Sung JH, Park KS, Park SG, Herpesvirus-associated ubiquitin-specific protease (HAUSP) modulates peroxisome proliferator-activated receptor gamma (PPARgamma) stability through its deubiquitinating activity. The Journal of biological chemistry 288, 32886–32896 (2013); published online EpubNov 15 (10.1074/jbc.M113.496331). [PubMed: 24072712]
34. Lee KM, Yang SJ, Kim YD, Choi YD, Nam JH, Choi CS, Choi HS, Park CS, Disruption of the cereblon gene enhances hepatic AMPK activity and prevents high-fat diet-induced obesity and insulin resistance in mice. Diabetes 62, 1855–1864 (2013); published online EpubJun (10.2337/db12-1030). [PubMed: 23349485]
35. Li P, Song Y, Zan W, Qin L, Han S, Jiang B, Dou H, Shao C, Gong Y, Lack of CUL4B in Adipocytes Promotes PPARgamma-Mediated Adipose Tissue Expansion and Insulin Sensitivity. Diabetes 66, 300–313 (2017); published online EpubFeb (10.2337/db16-0743). [PubMed: 27899484]
36. Foletta VC, White LJ, Larsen AE, Leger B, Russell AP, The role and regulation of MAFbx/atrogin-1 and MuRF1 in skeletal muscle atrophy. Pflugers Archiv : European journal of physiology 461, 325–335 (2011); published online EpubMar (10.1007/s00424-010-0919-9). [PubMed: 21221630]
37. Rom O, Reznick AZ, The role of E3 ubiquitin-ligases MuRF-1 and MAFbx in loss of skeletal muscle mass. Free radical biology & medicine 98, 218–230 (2016); published online EpubSep (10.1016/j.freeradbiomed.2015.12.031). [PubMed: 26738803]
38. Katafuchi T, Holland WL, Kollipara RK, Kittler R, Mangelsdorf DJ, Kliewer SA, PPARgamma-K107 SUMOylation regulates insulin sensitivity but not adiposity in mice. Proceedings of the National Academy of Sciences of the United States of America 115, 12102–12111 (2018); published online EpubNov 27 (10.1073/pnas.1814522115). [PubMed: 30420515]
39. Zhang Y, Shao J, Wang Z, Yang T, Liu S, Liu Y, Fan X, Ye W, Growth differentiation factor 11 is a protective factor for osteoblastogenesis by targeting PPARgamma. Gene 557, 209–214 (2015); published online EpubFeb 25 (10.1016/j.gene.2014.12.039). [PubMed: 25534870]
40. Yang J, Qian J, Wezeman M, Wang S, Lin P, Wang M, Yaccoby S, Kwak LW, Barlogie B, Yi Q, Targeting beta2-microglobulin for induction of tumor apoptosis in human hematological malignancies. Cancer cell 10, 295–307 (2006); published online EpubOct (10.1016/j.ccr.2006.08.025). [PubMed: 17045207]
41. Liu Z, Xu J, He J, Liu H, Lin P, Wan X, Navone NM, Tong Q, Kwak LW, Orlowski RZ, Yang J, Mature adipocytes in bone marrow protect myeloma cells against chemotherapy through autophagy activation. Oncotarget 6, 34329–34341 (2015); published online EpubOct 27 (10.18632/oncotarget.6020). [PubMed: 26455377]
42. Roodman GD, Treatment strategies for bone disease. Bone Marrow Transplant 40, 1139–1146 (2007); published online EpubDec (1705802 [pii] 10.1038/sj.bmt.1705802). [PubMed: 17680018]
43. Zwerina J, Hayer S, Redlich K, Bobacz K, Kollias G, Smolen JS, Schett G, Activation of p38 MAPK is a key step in tumor necrosis factor-mediated inflammatory bone destruction. Arthritis and rheumatism 54, 463–472 (2006); published online EpubFeb (10.1002/art.21626). [PubMed: 16447221]
44. Yang J, He J, Wang J, Cao Y, Ling J, Qian J, Lu Y, Li H, Zheng Y, Lan Y, Hong S, Matthews J, Starbuck MW, Navone NM, Orlowski RZ, Lin P, Kwak LW, Yi Q, Constitutive activation of p38 MAPK in tumor cells contributes to osteolytic bone lesions in multiple myeloma. Leukemia 26, 2114–2123 (2012); published online EpubSep (10.1038/leu.2012.71). [PubMed: 22425892]
45. Bam R, Khan S, Ling W, Randal SS, Li X, Barlogie B, Edmondson R, Yaccoby S, Primary myeloma interaction and growth in coculture with healthy donor hematopoietic bone marrow.

BMC cancer 15, 864 (2015); published online EpubNov 6 (10.1186/s12885-015-1892-7). [PubMed: 26545722]

46. Liu Z, Xu J, He J, Zheng Y, Li H, Lu Y, Qian J, Lin P, Weber DM, Yang J, Yi Q, A critical role of autocrine sonic hedgehog signaling in human CD138+ myeloma cell survival and drug resistance. Blood 124, 2061–2071 (2014); published online EpubSep 25 (10.1182/blood-2014-03-557298). [PubMed: 25049282]

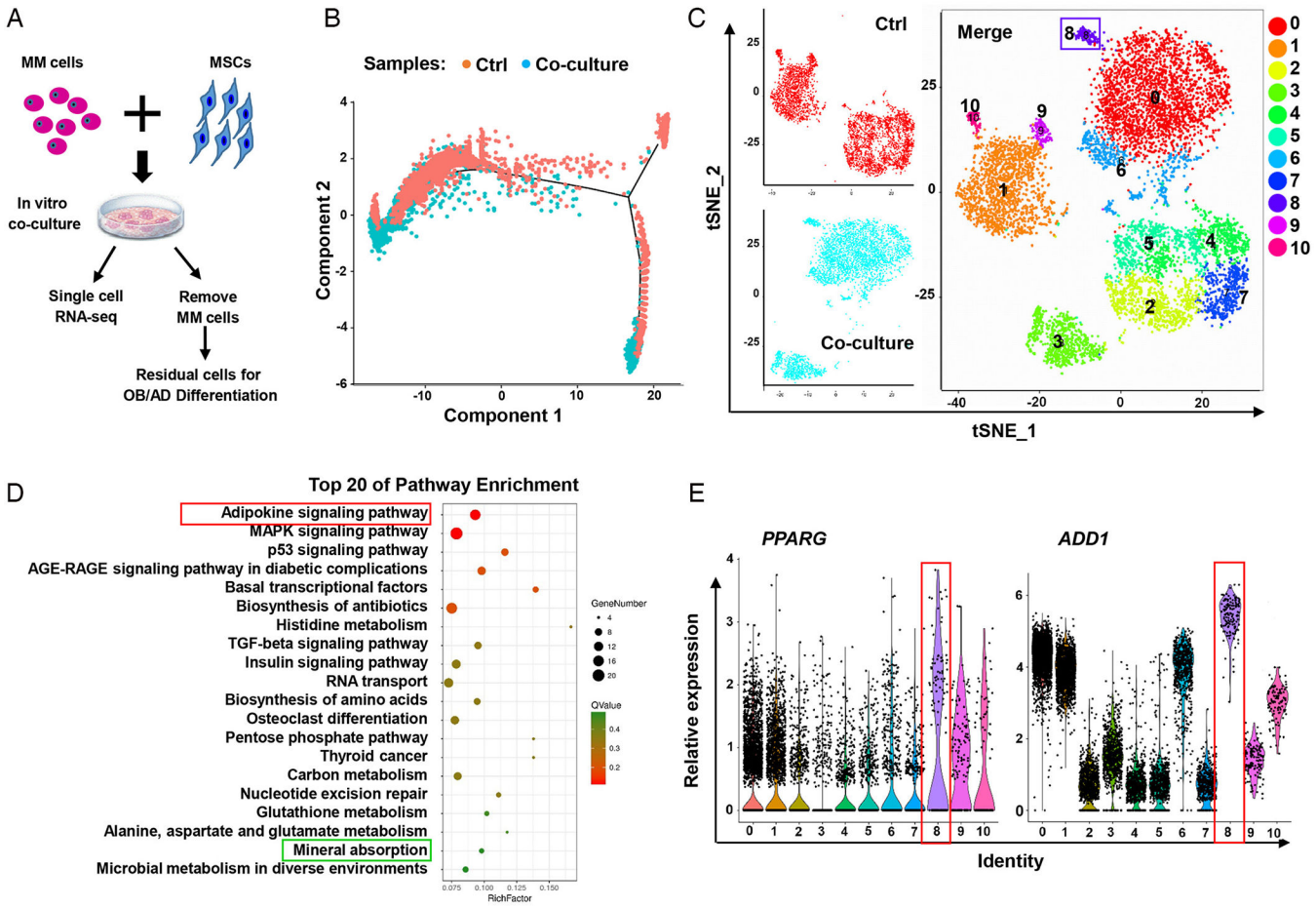

Fig. 1. scRNA-seq reveals the lineage determination of human MSCs co-cultured with myeloma cells.

(**A**) System for co-culturing of human MSCs with the human multiple myeloma cell (MM) line MM.1S in a 1:1 mixture of adipocyte (AD) and osteoblast (OB) medium. Cell were co-cultured for 48 hours then MSC-derived cells were subjected to single-cell RNA sequencing (scRNA-seq). As a control, scRNA-seq was also performed on MSCs cultured alone in 1:1 AD:OB medium. (**B**) The single-cell trajectory reconstructed by Monocle in the control (Ctrl) and co-culture (Coculture) groups. Each point represents a cell, and colors indicate their respective group. $n = 2$ independent experiments. The trajectory constructed by Monocle is in black. (**C**) T-distributed stochastic neighbor embedding (t=SNE) plot depicting clusters of MSCs cultured alone (Ctrl) or co-cultured with MM cells. The first two dimensions are shown. Each cluster represents individual cells with similar transcriptional profiles of MSCs or different MSC lineages, with total of 10 clusters from aggregated samples of 2 biologically independent experiments. (**D**) Enrichment analysis showing the 20 most significantly changed pathways in the MSCs co-cultured with MM cells. Red indicates activated pathways, and green indicates repressed pathways. (**E**) Distributions of unique transcripts per cell and *PPARG* and *CEBPB* gene expression in all cell clusters. The red frame shows the highest expression among the clusters.

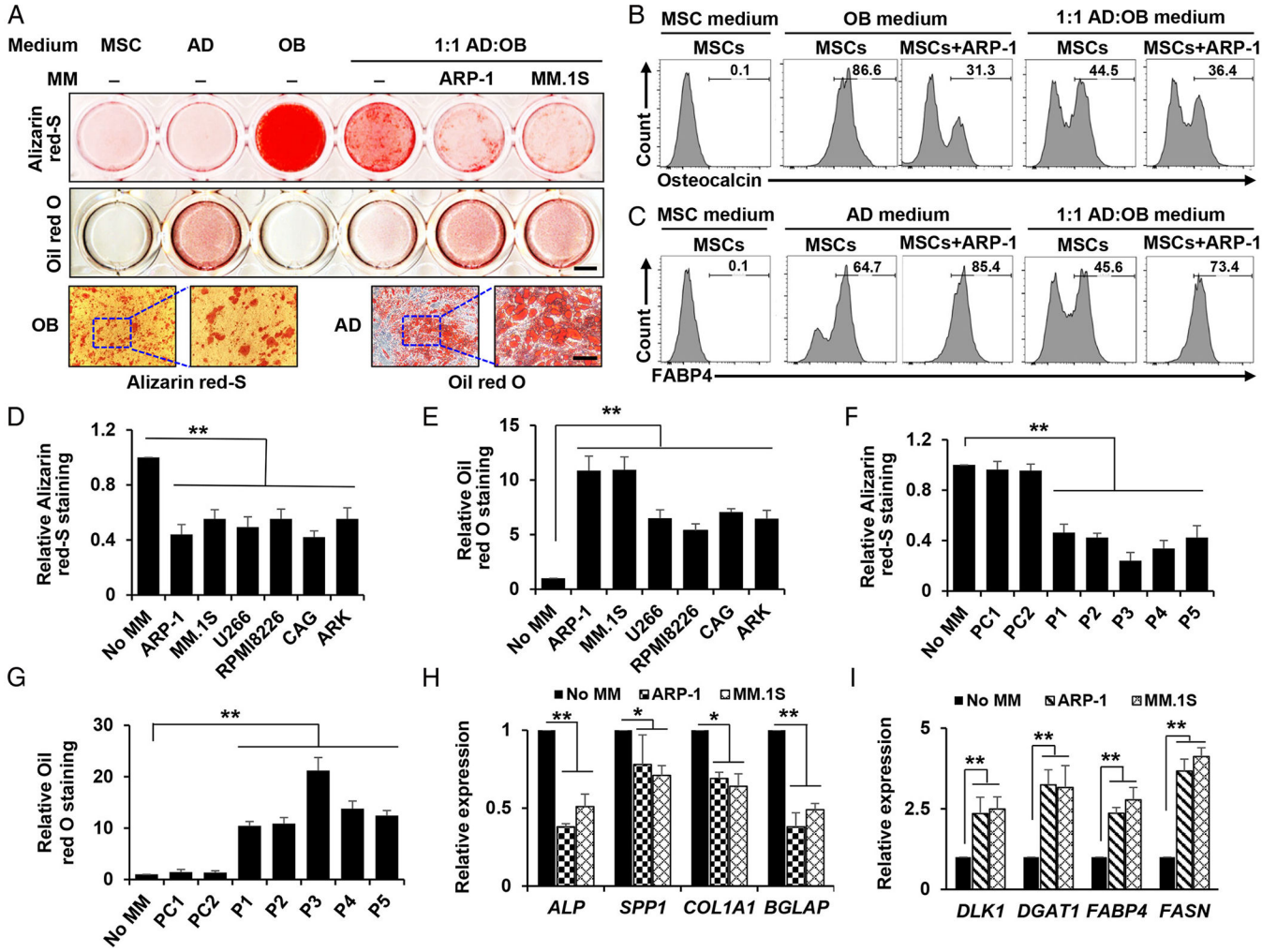

Fig. 2. Co-culture with myeloma cells induces MSC differentiation into adipocytes rather than osteoblasts.

(**A**) Representative images of Alizarin red-S and Oil red O staining (whole wells and enlarged views) of MSCs cultured alone or co-cultured with ARP-1 or MM.1S myeloma cell lines in MSC medium, adipocyte (AD) medium, osteoblast (OB) medium, or mixed 1:1 AD:OB medium as indicated. $n = 3$ independent experiments. Scale bar, 5 mm (whole wells), 20 μm (enlargements). (**B** and **C**) Flow cytometric analysis showing the percentage of osteocalcin$^+$ (B) and FABP4$^+$ (C) cells in cultures of MSCs alone or in direct contact with ARP-1 cells in the indicated medium. Data are representative of 3 independent experiments with each sample analyzed in triplicate. (**D** and **E**) Quantification of Alizarin red-S (D) and Oil red O (E) staining of MSCs cultured alone (No MM) or co-cultured with the six indicated myeloma cell lines. Combined data are from 3 biologically independent experiments. (**F** and **G**) Quantification of Alizarin red-S (F) and Oil red O (G) staining of MSCs cultured alone or co-cultured with primary myeloma cells isolated from bone marrow aspirates of five myeloma patients (P1–P5) or normal plasma cells from the bone marrow of two healthy donors (PC1 and PC2). Combined data are from $n = 3$ experiments using the same donor source material. (**H** and **I**) qRT-PCR showing the expression of the osteoblast

differentiation–associated genes *ALP*, *SPP1*, *COL1A1*, and *BGLAP* (H) and the adipocyte differentiation–associated genes *DLK1*, *DGAT1*, *FABP4*, and *FASN* (I) in cells generated by co-culture of MSCs with myeloma cells relative to expression of each gene in MSCs cultured alone. Combined data are from $n = 3$ independent experiments. All data are means ± SD. *$P \leq 0.05$; **$P \leq 0.01$. *P* values were determined using one-way ANOVA with Tukey's multiple comparisons test.

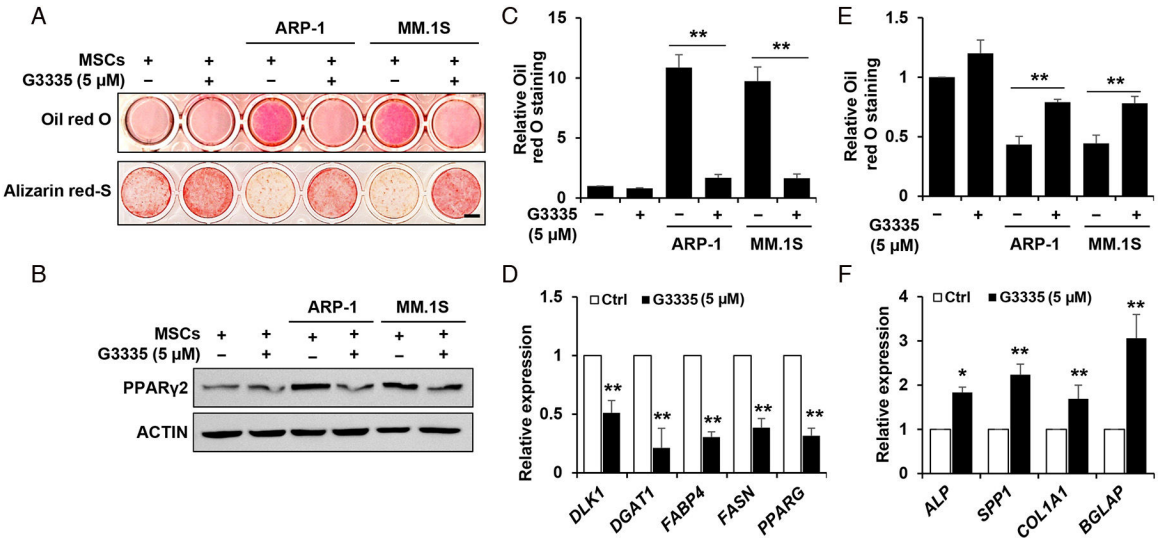

Fig. 3. Myeloma cells activate PPARγ2 in MSCs.

(**A**) Representative images of Oil red O or Alizarin red-S staining of MSCs cultured alone or co-cultured with ARP-1 or MM.1S myeloma cells in 1:1 OB:AD medium and treated with the PPARγ2 antagonist G3335 as indicated. Scale bar, 5 mm. (**B**) Representative Western blot for PPARγ2 in cells treated as in (A). Quantitation is presented in fig. S1. Actin is a loading control. (**C** to **F**) Quantitative analysis of Oil red O staining (C), adipocyte differentiation-associated gene expression (D), Alizarin red-S staining (E), and osteoblast differentiation-associated gene expression (F) in cells treated as in (A). Data are means ± SD from $n = 3$ independent experiments. *$P \leq 0.05$; **$P \leq 0.01$. P values were determined using student's t test for paired samples (D and F) and one-way ANOVA with Tukey's multiple comparisons test (C and E).

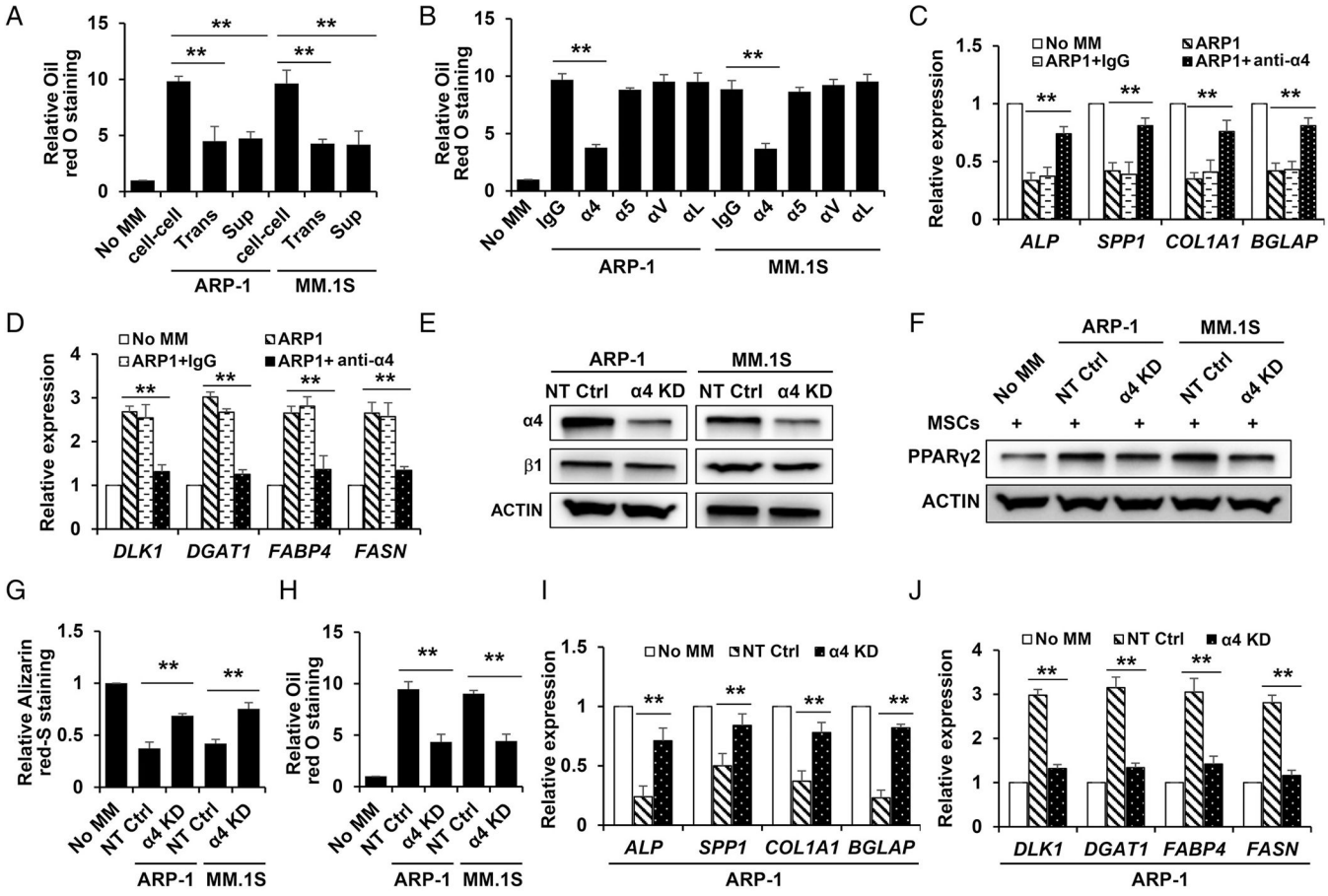

Fig. 4. Myeloma cell integrin α4 enhances PPARγ2 induction in MSCs and skews MSC differentiation.

(**A**) Oil red O staining in MSCs cultured alone (No MMs) or co-cultured with ARP-1 or MM.1S myeloma cells in 1:1 AD:OB medium directly (cell-cell) or separated by transwell inserts (Trans) or in myeloma cell culture media (sup). Staining was quantified relative to the No MM condition. Representative data are from 3 independent experiments. (**B to D**) Relative Oil red O staining (B) and the relative expression of the indicated osteoblast (C) and adipocyte (D) marker genes in MSCs cultured alone (No MM) or co-cultured with ARP-1 or MM.1S cells with or without neutralizing antibodies against integrin subunits α4, α5, αV, or αL. Combined data are from 3 independent experiments. (**E**) Western blot showing integrin α4 and integrin β1 in ARP-1 and MM.1S cells expressing shRNA targeting integrin α4 (α4 KD) or non-targeted control shRNAs (NT Ctrl). Actin is a loading control. (Blot is a representative of 3 independent experiments, and blot quantitation data is presented in fig. S2C. F **to** J) PPARγ2 protein (F), Alizarin red-S staining (G), Oil red O staining (H), osteoblast marker gene expression (I), and adipocyte marker gene expression (J) in MSCs cultured alone or co-cultured with ARP-1 or MM.1S cells expressing NT Ctrl or α4 KD shRNA. Blots in (E and F) are representative of 3 independent experiments, and blot quantitation is presented in fig. S2A and S2D, respectively. Data in (G to J) are means ± SD from $n = 3$ independent experiments using MSCs derived from BM aspirates of three

healthy donors. Data are $^{**}P \leq 0.01$. *P* values were determined using one-way ANOVA with Tukey's multiple comparisons test.

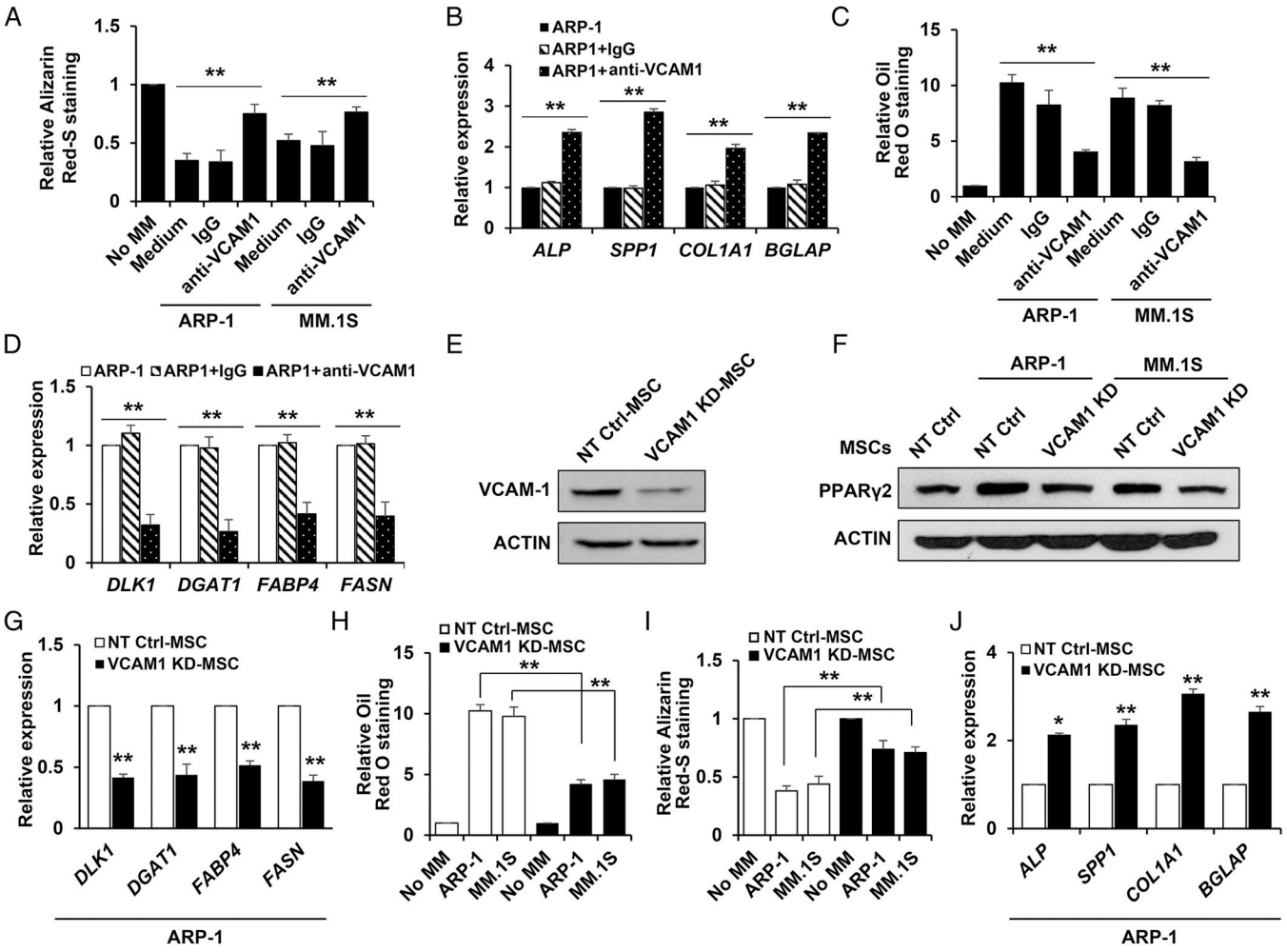

Fig. 5. VCAM1 mediates myeloma-induced PPARγ2 activation and MSC differentiation.

(**A** to **D**) Alizarin red-S staining (A), Oil red O staining (B), and real-time PCR analysis of the expression of osteoblast (C) and adipocyte (D) marker genes in MSCs cultured alone (No MM) or co-cultured with ARP-1 or MM.1S myeloma cells in the presence of a neutralizing antibody against VCAM1 or IgG (control). Data are from $n = 3$ independent experiments. (**E**) Western blotting analysis showing VCAM1 in the MSCs infected with a lentivirus carrying non-targeted control shRNAs (NT Ctrl-MSCs) or human VCAM1 shRNAs (VCAM1 KD-MSCs). Actin is a loading control. Blot is a representative of 3 independent experiments, and blot quantitation is presented in fig. S3A. (F **to** J) PPARγ2 protein (F), adipocyte gene expression (G), Oil red O staining (H), Alizarin red-S staining (I), and osteoblast gene expression (J) in MSCs expressing NT Ctrl or VCAM1 shRNAs co-cultured with ARP-1 or MM.1S cells in 1:1 OB:AD medium. Blot in (F) is a representative of 3 independent experiments, and blot quantitation is presented in fig. S3B. Data are means ± SD from $n = 3$ independent experiments. $^{*}P \leq 0.05$; $^{**}P \leq 0.01$. *P* values were determined using one-way ANOVA with Tukey's multiple comparisons test except in (G) and (J), where student's *t* test for paired samples were used.

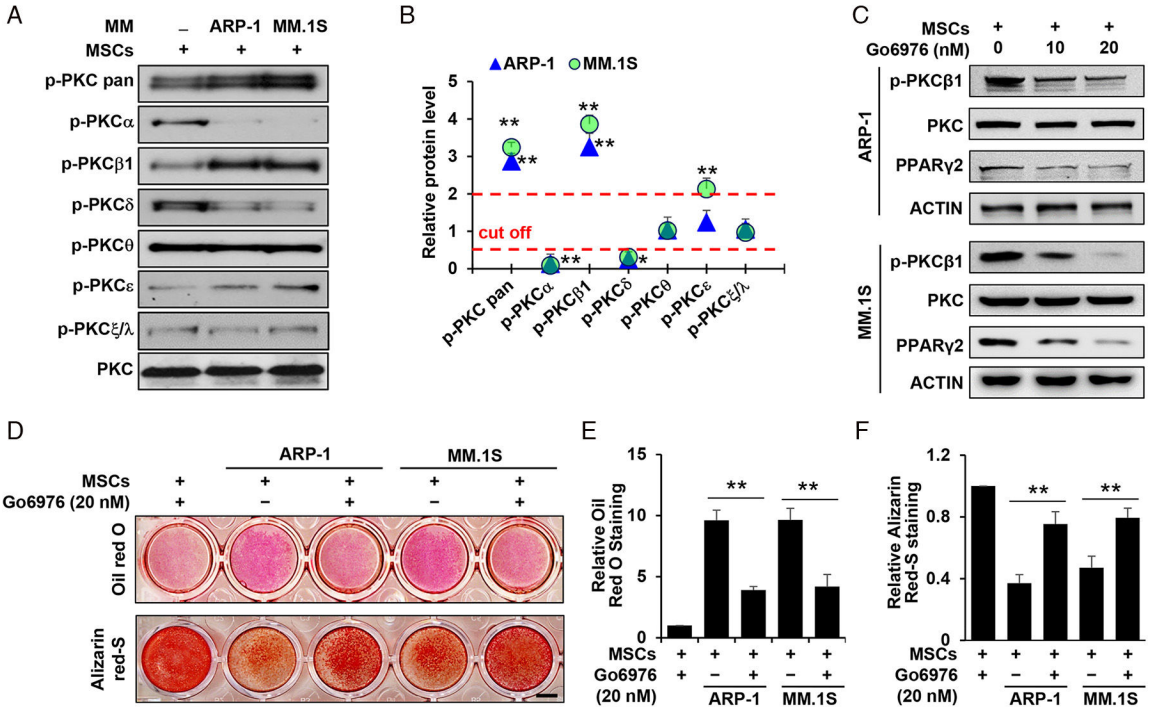

Fig. 6. Myeloma cells activate PPARγ2 and shift the fate of MSCs through the PKCβ1 signaling pathway.

(**A**) Western blotting for showing all phosphorylated PKCs (p-PKC pan), the indicated phosphorylated (p-) PKC isoforms, and total PKC in MSCs cultured alone or co-cultured with ARP-1 or MM.1S myeloma cells. The abundances of total PKC served as protein loading controls. (**B**) Quantification of the phosphorylation of PKC isoforms in MSCs co-cultured with myeloma cells in (A) relative to the MSC-only control. The cut-off values are fold change more than 2-fold or less than 0.5-fold. (**C**) Western blotting for phosphorylated PKCβ1, total PKC, and PPARγ2 in MSCs co-cultured with ARP-1 or MM.1S cells in the presence of the PKC inhibitor Go6976 or DMSO (control). Actin is a loading control. Blot is a representative of 3 independent experiments, and blot quantitation is presented in fig. S4. (**D**) Representative images of Oil red O staining and Alizarin red-S staining of MSCs cultured alone or co-cultured with ARP-1 or MM.1S myeloma cells in the presence of the PKC inhibitor Go6976 or DMSO (control). Scale bar, 5 mm. (E and F) Quantification of Oil red O staining (E) and Alizarin red-S staining (F), in cells treated as in (D). Data are means ± SD from $n = 3$ independent experiments. *$P \leq 0.05$; **$P \leq 0.01$. P values were determined using one-way ANOVA with Tukey's multiple comparisons test.

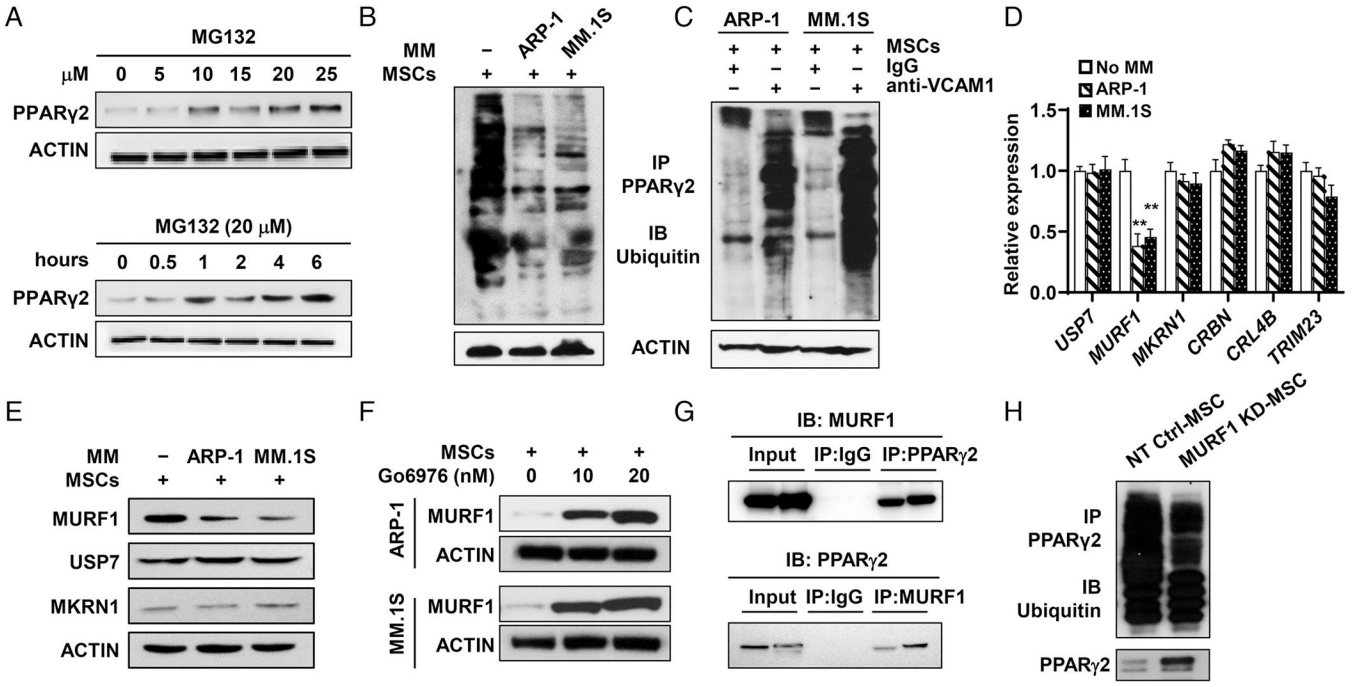

Fig. 7. Interaction with myeloma cells reduces the ubiquitylation of PPARγ2 in MSCs by decreasing MURF1.

(**A**) Western blotting analysis for PPARγ2 in MSCs cultured in 1:1 OB:AD medium and treated with the proteasome inhibitor MG132 for the indicated amounts of time. Actin is a loading control. (**B**) Immunoblotting (IB) for ubiquitin in PPARγ2 immunoprecipitates (IP) from MSCs cultured alone or co-cultured with ARP-1 or MM.1S myeloma cells in the presence of MG132. (**C**) Western blotting for ubiquitin in PPARγ2 immunoprecipitates from MSCs co-cultured with ARP-1 or MM.1S cells in the presence of MG132 and an antibody against VCAM1 or IgG (control). (**D**) Expression of the E3 ligase–encoding genes *USP7, MURF1, MKRN1, CRBN, CRL4B,* and *TRIM23* in MSCs co-cultured with myeloma cells relative to the expression in MSCs cultured alone (No MM). Data are means ± SD from $n = 3$ independent experiments. $^{**}P \leq 0.01$. *P* values were determined using one-way ANOVA with Tukey's multiple comparisons test. (**E**) Western blotting for USP7, MURF1, and MKRN1 in MSCs cultured alone or co-cultured with myeloma cells. (**F**) Western blotting for MURF1 in MSCs co-cultured with ARP-1 or MM.1S myeloma cells and treated with Go6976 or DMSO (control) as indicated. (**G**) Immunoblotting for MURF1 or PPARγ2 in PPARγ2 or MURF1 immunoprecipitates, respectively, from MSCs. IgG immunoprecipitates and whole cell lysate (input) were used as controls. (**H**) Immunoblotting for ubiquitin in PPARγ2 immunoprecipitates from MSCs expressing non-target control (NT Ctrl) or MURF1 shRNAs in the presence of MG132. Each blot is representative of $n = 3$ independent experiments, and blot quantitation is presented in fig. S5.

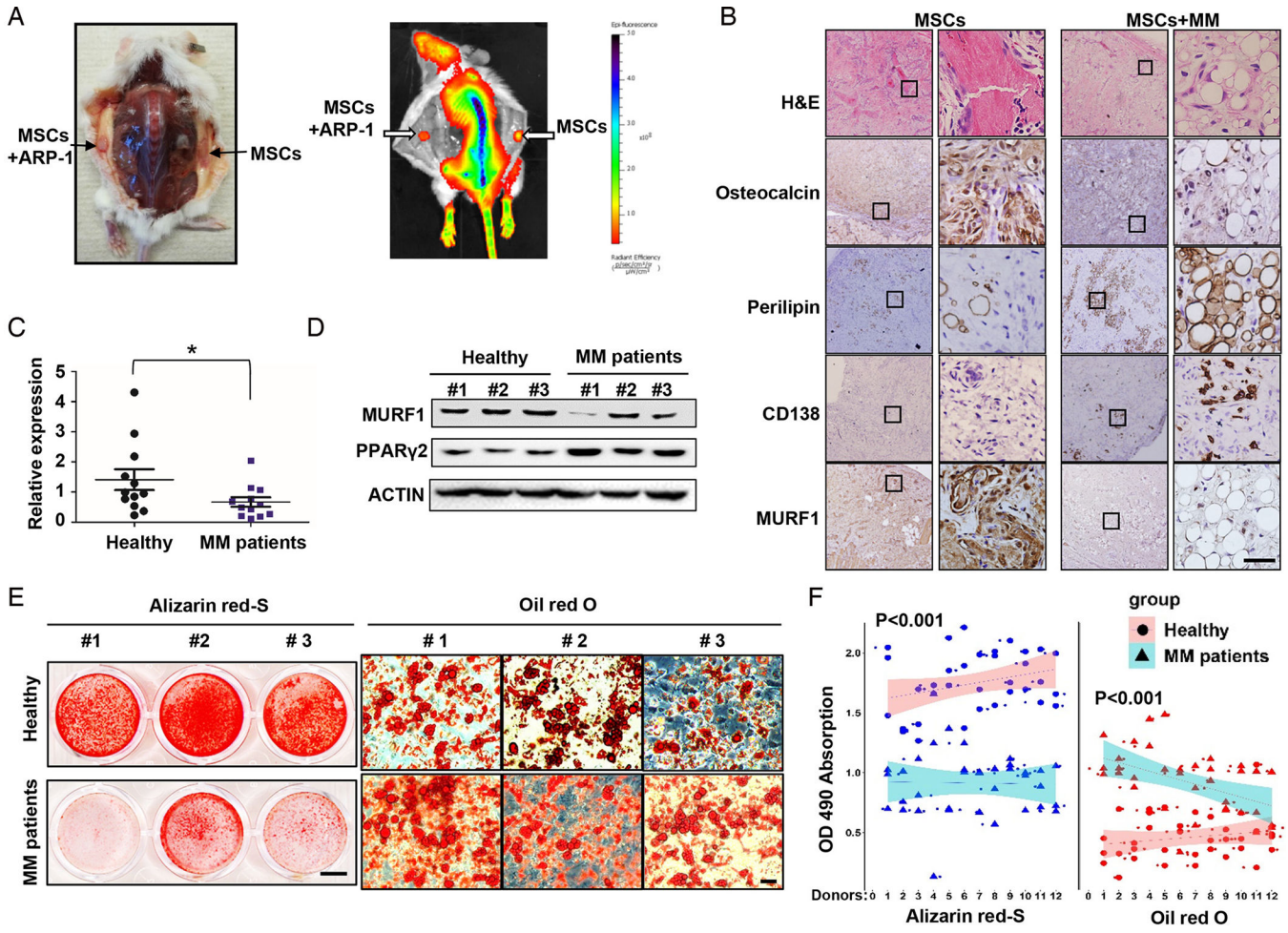

Fig. 8. Myeloma cells suppress osteoblast-mediated bone formation and promote adipogenesis through decreasing MURF1 in MSCs in vivo.

(**A**) Representative images of subcutaneous tissues and bone density in mice implanted with human MSCs plus ECFCs in the right flank and MSCs plus ECFCs mixed with ARP-1 myeloma cells in the left flank. The arrows indicate bone formation in subcutaneous tissue, and the bars indicate bone density. (**B**) Representative H&E and immunohistochemical staining for the osteoblast marker osteocalcin, the adipocyte marker perilipin, the myeloma cell marker $CD138^{+}$, and MURF1 of the subcutaneous tissues from (A). Scale bar, 20 μm. Data represent $n = 3$ independent experiments with 5 mice each. (**C**) Expression of *MURF1* in MSCs from BM aspirates from 12 myeloma patients and 12 age-matched healthy donors relative to expression in a randomly selected sample from healthy donor. Data are from $n = 3$ experiments using the same donor source material. $^{*}P \leq 0.05$. *P* values were determined using student's *t* test. (**D** to **E**) Western blotting for MURF1 and PPARγ2 (D) and Alizarin red-S and Oil red O staining (E) in MSCs from BM aspirates from three healthy donors and three myeloma patients. Blot and images are representative of three experiments using the same donor materials, and blot quantitation is presented in fig. S6. Scale bar, 5 mm (whole wells), 100 μm (enlargements). (**F**) Quantitation of Alizarin red-S and Oil red O staining in the cultures of MSCs from BM aspirates from healthy donors and myeloma patients in (C).

Data are from $n = 3$ experiments using the same donor source material. P values were determined using student's t test.